Potential energy functions of the $\tilde{X}^2B_1$, $\tilde{A}^2B_2$, $\tilde{B}^2A_1$, and $\tilde{C}^2A_2$ states of Cl_2O^+ and the $\tilde{X}^1A_1$ state of Cl_2O: Franck–Condon simulations of photoelectron bands of Cl_2O which include anharmonicity

Foo-Tim Chau[a)]
Department of Applied Biology and Chemical Technology, Hong Kong Polytechnic University, Hung Hom, Hong Kong

John M. Dyke
Department of Chemistry, University of Southampton, Highfield, Southampton SO17 1BJ, United Kingdom

Edmond P. F. Lee[b)] and Daniel Kam-Wah Mok[a)]
Department of Applied Biology and Chemical Technology, Hong Kong Polytechnic University, Hung Hom, Hong Kong

(Received 24 September 2002; accepted 4 December 2002)

Restricted-spin coupled-cluster single and double plus perturbative triple excitations [RCCSD (T)] and/or complete-active-space self-consistent-field multireference internally-contracted configuration interaction (CASSCF/MRCI) potential energy functions of the $\tilde{X}^2B_1$, $\tilde{A}^2B_2$, $\tilde{B}^2A_1$, and $\tilde{C}^2A_2$ states of Cl_2O^+ and the $\tilde{X}^1A_1$ state of Cl_2O, with basis sets of up to the augmented-correlation-consistent-polarized-valence-quadruple-zeta quality, have been reported. For each of these states, vibrational wave functions of the symmetric stretching and bending modes have been computed, employing the potential energy function obtained at the highest level of calculation, with Watson's Hamiltonian and anharmonic vibrational wave functions expressed as linear combinations of harmonic basis functions. The helium I photoelectron spectrum of Cl_2O has been simulated with Franck–Condon factors calculated using computed anharmonic vibrational wave functions and allowing for Duschinsky rotation. The adiabatic ionization energies (AIEs) to the four lowest cationic states of Cl_2O^+ have been evaluated at the RCCSD(T) level with basis sets of up to polarized-valence-quintuple-zeta quality and by various extrapolation techniques to the basis set limit. Revised equilibrium geometrical parameters of the $\tilde{X}^2B_1$ and $\tilde{C}^2A_2$ states of Cl_2O^+ were obtained from the iterative Franck–Condon analysis procedure, and revised AIEs for the $\tilde{A}^2B_2$ and $\tilde{B}^2A_1$ states of Cl_2O^+ were estimated based on comparison between the simulated and observed photoelectron spectra. It was found that inclusion of anharmonicity in the Franck–Condon factor calculations for each electronic state improves the quality of the simulated spectrum. The computed T_1 diagnostics from the RCCSD calculations suggest that the $\tilde{B}^2A_1$ state of Cl_2O^+, with the $\cdots(9a_1)^1(3b_2)^2(10a_1)^0$ electronic configuration, possesses multiconfigurational character in the region of $r(\mathrm{ClO})=1.87$ Å and $\theta(\mathrm{ClOCl})=125°$. CASSCF/MRCI/aug-cc-pVQZ(no g) calculations show an avoided crossing between the $\tilde{B}^2A_1$ state and $(2)^2A_1$ state [with the $\cdots(9a_1)^2(3b_1)^0(10a_1)^1$ electronic configuration], in the region of $1.96>r>1.80$ Å and $137.0>\theta>132.0°$. © *2003 American Institute of Physics.* [DOI: 10.1063/1.1540621]

I. INTRODUCTION

Recently, we reported *ab initio* calculations on the ground electronic state of Cl_2O and four low-lying cationic states of Cl_2O^+, and Franck–Condon simulations of the He I photoelectron (PE) spectrum of Cl_2O (Ref. 1) based on the harmonic oscillator model.[2] Subsequently, we published a combined experimental and computational study on the He I PE spectrum of F_2O.[3] The *ab initio* part of the later study on F_2O included energy scans on the symmetric stretching and bending surfaces, giving fitted potential energy functions (PEFs), which were employed in Franck–Condon factor (FCF) calculations which included the effects of anharmonicity. In this study of F_2O, it was found that, for the first photoelectron (PE) band, which was observed with well-resolved vibrational structure,[1] the simulated spectrum which included anharmonicity was significantly superior to that obtained based on the harmonic oscillator model, when compared with the experimental spectrum. In addition, it was found that the harmonic simulation of the second PE band of F_2O, corresponding to ionization to the $\tilde{A}^2B_2$ cationic state, gave a PE band of width almost double that obtained from the anharmonic simulation. In view of the considerable differences between simulated PE bands of F_2O obtained within the harmonic oscillator model and those obtained including anharmonicity, and the better agreement of the anharmonic simulated band envelopes with the experimental envelopes,

a)Author to whom correspondence should be addressed.
b)Also at: Department of Chemistry, University of Southampton, Highfield, Southampton SO17 1BJ, United Kingdom.

it was decided to study again the He I PES of Cl_2O by Franck–Condon simulations which include anharmonicity in each electronic state. In addition, the adiabatic ionization energies (AIEs) of the $\tilde{X}\,^2B_1$, $\tilde{A}\,^2B_2$, $\tilde{B}\,^2A_1$, and $\tilde{C}\,^2A_2$ states of Cl_2O^+ have been calculated by various extrapolation techniques to the complete basis set limit, and RCCSD(T)/aug-cc-pVQZ and/or CASSCF/MRCI/aug-cc-pVQZ(no *g*) PEFs of the electronic states considered are reported for the first time.

Since our previous investigation on the He I PES of Cl_2O was reported,[2] a number of theoretical studies on Cl_2O have appeared,[4–7] which focus mainly on the ground and excited states of Cl_2O, and/or its absorption spectrum. Relating to the Cl_2O^+ cation (for earlier works, see Refs. 1 and 2, and references therein), Ruhl *et al.*[8] published a photoionization mass spectrometry study on several oxides of chlorine. The Cl_2O ionization energies of 10.88 ± 0.02 and 12.74 eV obtained in this study for ionization to the $\tilde{X}\,^2B_1$ and $\tilde{C}\,^2A_2$ states of Cl_2O^+, respectively, are in excellent agreement with the AIEs measured in the He I PE spectrum.[1] Very recently, Hanel *et al.*[9] reported a combined electron impact and *ab initio* study on the ionization energies of Cl_2O and its dimer. Minimum-energy geometrical parameters of the ground states of Cl_2O and its cation were calculated at the MP2/6−311+G(2*df*) level, giving a first AIE of 11.15 eV. An AIE of 10.89 eV was also computed at the G3 (extrapolation) level.

During the preparation of the present manuscript, a spectral simulation study on the $\tilde{A}\,^2B_2\leftarrow\tilde{X}\,^1A_1$ and $\tilde{B}\,^2A_1\leftarrow\tilde{X}\,^1A_1$ PE bands of Cl_2O^+, based on the Lanczos method, has appeared.[10] This work by Mahapatra, which considers nonadiabatic effects at the conical intersection between the diabatic potential energy surfaces of the $\tilde{A}\,^2B_2$ and $\tilde{B}\,^2A_1$ states of Cl_2O^+, is of particular relevance to, and compliments, the present study. It will be discussed further in the last section of this paper. In brief, in Ref. 10, nonadiabatic coupling between the two electronic states was estimated by the linear vibronic coupling (LVC) scheme and the vibrational motion was treated within the harmonic oscillator model. Various parameters required in the vibronic Hamiltonian to calculate the potential energy functions were taken from either available experimental or *ab initio* studies, or computed by the outer-valence Green's function (OVGF) method. Certain parameters (λ, τ, and κ; see Ref. 10 for detail and also see later text) were adjusted in order to obtain the best match between the simulated and observed spectra. It was concluded that nonadiabatic coupling could affect the vibrational structure of the $\tilde{B}\,^2A_1\leftarrow\tilde{X}\,^1A_1$ PE band of Cl_2O^+ significantly, but it has a very small effect on the $\tilde{A}\,^2B_2\leftarrow\tilde{X}\,^1A_1$ PE band.

II. THEORETICAL CONSIDERATIONS AND COMPUTATIONAL DETAILS

A. *Ab initio* calculations

RCCSD(T) energy scans were carried out on the $\tilde{X}\,^2B_1$, $\tilde{A}\,^2B_2$, $\tilde{B}\,^2A_1$, and $\tilde{C}\,^2A_2$ states of Cl_2O^+ and the $\tilde{X}\,^1A_1$ state of Cl_2O, initially with the aug-cc-pVTZ basis set, along the symmetric stretching and bending coordinates. For the $\tilde{B}\,^2A_1$ state of Cl_2O^+, the computed T_1 diagnostics in the RCCSD(T) calculation were found to be rather large (>0.078) in the region of $r(\mathrm{ClO})=1.76-1.86$ Å and $\theta(\mathrm{ClOCl})=116°-132°$. At $r=1.867$ Å and $\theta=124.5°$, the ROHF calculation failed to converge after a large number of SCF iterations; thus it has to be concluded that the computed energy obtained from the subsequent RCCSD(T) calculation at this geometry is unreliable. All the above observations from the RCCSD(T)/aug-cc-pVTZ energy scans of the $\tilde{B}\,^2A_1$ state of Cl_2O^+ suggest that, very likely, a higher $^2A_1$ state is nearby and hence multi-reference character becomes important in this region of the $\tilde{B}\,^2A_1$ energy surface. In order to obtain a reliable PEF for the $\tilde{B}\,^2A_1$ state, CASSCF/MRCI/aug-cc-pVTZ energy scans were carried out. In these CASSCF/MRCI calculations (and also subsequent CASSCF/MRCI calculations discussed below), the full valence space was active, and the two lowest $^2A_1$ states were considered with equal weights in both the CASSCF and MRCI parts of the calculations.

Geometry optimization calculations were also carried out at the RCCSD(T)/cc-pVQZ level for all states of interest, with the aim of obtaining more reliable geometrical parameters to be employed in the subsequent Franck–Condon simulations. It was found that the equilibrium bond lengths, r_e's, obtained with the cc-pVQZ basis set differ by ≈0.01 Å from those obtained with the aug-cc-pVTZ basis set (from the PEFs) for most of the states studied (see later text). This rather large basis set effect on the computed r_e's led to doubt about of the reliability of the PEFs obtained using the aug-cc-pVTZ basis set. In view of this concern, RCCSD(T)/aug-cc-pVQZ energy scans were carried out for all the states considered, except for the $\tilde{B}\,^2A_1$ state, where CASSCF/MRCI/aug-cc-pVQZ(no *g*) energy scans were carried out. In these MRCI calculations, the numbers of uncontracted and contracted configurations are 563 and 2.74 millions, respectively. In the following text, we will focus on the PEFs obtained employing the aug-cc-pVQZ basis set and those obtained with the aug-cc-pVTZ basis set will not be discussed for the sake of simplicity.

AIEs were calculated systematically using the RCCSD(T) method with the series of cc-pV*X*Z basis sets, where $X=$ D, T, Q, and 5, at the respective RCCSD(T)/cc-pVQZ optimized geometries. The computed AIEs obtained with different basis sets were fitted to expressions of various extrapolation techniques to the basis set limit[11–14] (see below). In summary, it is the purpose of this present study to obtain equilibrium geometrical parameters, PEFs and AIEs at the near state-of-the-art levels of *ab initio* calculation. The PEFs were then used to calculate vibrational wave functions for subsequent Franck–Condon factors (FCF) calculations.

All the above calculations were performed with the MOLPRO suite of programs.[15]

B. Potential energy functions, anharmonic vibrational wave functions, and Franck–Condon factor calculations

For each electronic state involved in the ionization process, the potential energy function (PEF), V, was determined

by fitting the following polynomial to an appropriate number of RCCSD(T)/aug-cc-pVQZ or CASSCF/MRCI/aug-cc-pVQZ(no *g*) single point energies,

$$V=\sum_{ij} C_{ij}(S_1)^i(S_2)^j+V_{\mathrm{eqm}}. \quad (1)$$

In this equation, the PEFs are expressed as displacements of symmetry coordinates

$$S_1=(\Delta r_1+\Delta r_2)/\sqrt{2},$$

and the bending coordinates suggested by Carter and Handy,[16]

$$S_2=\Delta\theta+\alpha\Delta\theta^2+\beta\Delta\theta^3,$$

where $\Delta r_{1,2}$ and $\Delta\theta$ are displacements in the r(ClO) bond lengths (for the symmetric stretch, $\Delta r_1=\Delta r_2$) and in the θ(ClOCl) bond angle from the corresponding equilibrium values, respectively. By restricting the energy gradient in S_2 to zero when the molecule is linear (i.e., when $\theta=\pi$), an expression relating α and β can be obtained,

$$\beta=[1+3\alpha(\pi-\theta_{\mathrm{eqm}})^2]/[-2(\pi-\theta_{\mathrm{eqm}})].$$

The nonlinear least squares fit procedure,[17] NL2SOL, was employed to obtain the C_{ij}'s, V_{eqm}, r_{eqm}, θ_{eqm}, α, and β from the computed single point energy data. The asymmetric stretching mode has been ignored, because the observed bands in the He I PE spectrum do not show any identifiable vibrational structure associated with the asymmetric stretching mode.[1] In addition, the computed FCFs involving the asymmetric stretching mode, based on the harmonic oscillator model, have negligible relative intensities.[2]

Terms of up to the fourth order and also the C_{05}, C_{06}, C_{50}, and C_{60} terms were included in the PEF [Eq. (1)] for all states considered. The energy grid points cover the ranges of $\Delta r=\pm 0.3$ Å and $\Delta\theta=\pm 30°$ for the $\tilde{X}\,^1A_1$ state of Cl_2O, $0.15\leqslant\Delta r\leqslant 0.25$ Å and $\Delta\theta=\pm 30°$ for the $\tilde{X}\,^2B_1$, $\tilde{A}\,^2B_2$, and $\tilde{B}\,^2A_1$ states, and $\Delta r=\pm 0.25$ Å and $\Delta\theta=\pm 18°$ for the $\tilde{C}\,^2A_2$ of Cl_2O^+.

Variational calculations, which employed the rovibronic Hamiltonian for a nonlinear molecule of Watson,[18] were carried out to obtain the anharmonic vibrational wave functions. The latter were expressed as linear combinations of harmonic oscillator functions, $h(v_1,v_2)$, where v_1 and v_2 denote the quantum numbers of the harmonic basis functions for the symmetric stretching and bending mode, respectively (see Refs. 3 and 19 for details). Harmonic basis functions, up to $h(10,10)$ with the restriction of $v_1+v_2<10$, were employed in the variational calculation of the neutral ground electronic state of Cl_2O. For the $\tilde{X}\,^2B_1$ and $\tilde{C}\,^2A_2$ cationic states, which have dominant structure in the stretching mode in their PE bands, harmonic basis functions of up to $h(20,15)$ with the restriction of $v_1+v_2<20$ were used. For the $\tilde{A}\,^2B_2$, and $\tilde{B}\,^2A_1$ cationic states, which have extensive bending progressions in the observed PE bands, a larger harmonic basis of $h(20,25)$ with $v_1+v_2<25$ was used in each case.

For each PE band, FCFs were computed employing the anharmonic vibrational wave functions and allowing for Duschinsky rotation, as described previously (see Refs. 19 and 20, and references therein). The iterative-Franck–Condon-analysis (IFCA) procedure, where the geometry change on ionization was varied around the best *ab initio* computed geometry change, while the geometrical parameters of the neutral Cl_2O molecule were fixed at the available experimental values,[21,22] was carried out to obtain the best match between the simulated and experimental spectra. A Gaussian function with a full-width-at-half-maximum of 20 meV was used in the simulated band for each vibrational component.

TABLE I. The RCCSD(T)/aug-cc-pVQZ potential energy functions of the $\tilde{X}\,^1A_1$ state of Cl_2O and the $\tilde{X}\,^2B_1$, $\tilde{A}\,^2B_2$, and $\tilde{C}\,^2A_2$ states of Cl_2O^+, and the CASSCF/MRCI/aug-cc-pVQZ(no *g*) potential energy function of the $\tilde{B}\,^2A_1$ state of Cl_2O^+.

Coefficients[a]	$\tilde{X}\,^1A_1$	$\tilde{X}\,^2B_1$	$\tilde{A}\,^2B_2$	$\tilde{B}\,^2A_1$	$\tilde{C}\,^2A_2$
C_{20}	0.4135	0.5651	0.4502	0.4653	0.3808
C_{11}	0.1043	0.1225	0.1979	0.1146	0.0773
C_{02}	0.1439	0.1462	0.1878	0.0870	0.1247
C_{30}	−0.5498	−0.8675	−0.5853	−0.9162	−0.4809
C_{21}	−0.2413	−0.2599	−0.3763	−0.2166	−0.1844
C_{12}	−0.2224	−0.2032	−0.5379	−0.1164	−0.2358
C_{03}	0.0301	0.0283	−0.2001	−0.0227	0.0103
C_{40}	0.4648	0.7114	0.4710	0.1506	0.4005
C_{22}	0.1111	0.0810	0.4518	−0.0655	0.1690
C_{04}	0.0832	0.0805	0.1955	0.0396	0.1072
C_{31}	0.0372	0.0816	0.3373	0.1061	0.0645
C_{13}	0.2176	0.2124	0.3317	0.0883	0.2254
C_{05}	0.2077	0.1353	0.1192	0.1057	0.0544
C_{06}	0.4703	0.2239	−0.1408	0.1723	0.0436
C_{50}	−0.3837	−0.1111	−0.3337	4.9583	−0.3483
C_{60}	0.2219	−0.2195	0.2959	−7.5709	0.2279
R_e/Å	1.7045	1.6335	1.7054	1.6522	1.7254
θ_e/°	110.81	117.53	90.84	132.30	107.36
α/rad^{-1}	0.0563	0.0006	0.0041	−0.2275	0.0256

[a]See text.

III. RESULTS AND DISCUSSION

A. PEFs and the two lowest $^2A_1$ states

The PEFs obtained at the highest level of calculation for the electronic states studied are given in Table I. The root mean square (rms) deviation of the fitted potentials from the computed single point energies are below 10 cm^{-1} for the RCCSD(T)/aug-cc-pVQZ PEFs. For the CASSCF/MRCI/aug-cc-pVQZ(no *g*) PEF of the $\tilde{B}\,^2A_1$ state, the rms deviation is 20 cm^{-1}. The slightly larger rms deviation of the MRCI PEF of the $\tilde{B}\,^2A_1$ state is very likely due to the influence of an avoided crossing between the $\tilde{B}\,^2A_1$ state, with the electronic configuration of $\cdots(9a_1)^1(3b_1)^2$, and the $(2)^2A_1$ state, with the electronic configuration of $\cdots(9a_1)^2(3b_1)^0(10a_1)^1$, near the region of $1.96>r(\mathrm{ClO})>1.80$ Å and $137.0>\theta(\mathrm{ClOCl})>132.0°$. At $r=1.96$ Å and $\theta=132.0°$, the computed MRCI energy of the $\tilde{B}\,^2A_1$ state is 306 cm^{-1} lower than that of the $(2)^2A_1$ state, but on including the Davidson correction for quadruple excitations, the MRCI+D energy of the $\tilde{B}\,^2A_1$ state is 88 cm^{-1} higher than that of the $(2)^2A_1$ state, suggesting an avoided crossing at the MRCI+D level of calculation. (MRCI+D energies were employed in the fitting of the PEF of the $\tilde{B}\,^2A_1$ state.) At this

geometry, the two lowest $^2A_1$ states are closest in energy among all the single point energy calculations considered in the present study. While the computed CI coefficient of the $\cdots(9a_1)^1(3b_1)^2$ configuration in the MRCI wave function at this geometry is 0.8282, the sum of the CI coefficients of all reference configurations for the $\tilde{B}\,^2A_1$ state is 0.9324. The closeness of the latter value to unity indicates that the reference configuration space of the MRCI wave function of the $\tilde{B}\,^2A_1$ state is adequate in this region, where the strongest configuration interaction between the two states is present. The interaction between these two $^2A_1$ states was further investigated and its effect on the observed PE spectrum will be discussed later. It suffices here to conclude that the CASSCF/MRCI calculations on the $\tilde{B}\,^2A_1$ state are adequate for the region covered by the energy scan carried out in the present study.

For the fitted PEF of the $\tilde{B}\,^2A_1$ state, it is noticed that the magnitudes of C_{50} and C_{60} are significantly larger than those of other coefficients in the PEF and C_{60} is negative (see Table I). Including higher order terms of the stretching mode, such as C_{70} and C_{80}, in the PEF reduces the magnitudes of C_{50} and C_{60} in the fitting, but the magnitudes of C_{70} and C_{80} are even larger than those of C_{50} and C_{60} shown in Table I and C_{80} is negative. The effects of these higher order terms on the fitted PEF are mainly in the long $r(\mathrm{ClO})$ region and the negative C_{60} or C_{80} terms have the effect of reducing the energy increases in the large $r(\mathrm{ClO})$ region, i.e., flattening the energy surface at large $r(\mathrm{ClO})$. All these observations suggest a larger anharmonic effect on the energy surface at the large $r(\mathrm{ClO})$ region than near the equilibrium geometry region. This larger anharmonic effect is almost certainly due to the avoided crossing discussed above. Nevertheless, within the scanned region, the deviations of the fitted PEF given in Table I from the computed *ab initio* energies are acceptably small and evenly distributed over the whole scanned surface. It is therefore concluded that the PEF reported here for the $\tilde{B}\,^2A_1$ state of Cl_2O^+ should be reliable within the scanned region, though it is expected to be inadequate outside the scanned region beyond the avoided crossing. In summary, despite the influence of the $(2)^2A_1$ state on a certain region of the energy surface of the $\tilde{B}\,^2A_1$ state, the CASSCF/MRCI/aug-cc-pVQZ(no *g*) PEF of the $\tilde{B}\,^2A_1$ state reported here should be reasonably reliable within the energy scanned region and adequate for the purpose of being employed to generate vibrational wave functions, which are used in subsequent FCF calculations.

The $(2)^2A_1$ state was characterized further by CIS(*n* states=15)/6-311+G(2*d*) geometry optimization and vibrational frequency calculations, employing the Gaussian suite of programs.[23] The geometry of the $(2)^2A_1$ state is optimized at $r=2.572$ Å and $\theta=106.3°$ and is a true minimum [the calculated harmonic vibrational frequencies are 506(a_1), 178(a_1), and 563(b_2) cm^{-1}]. At this geometry, the $(1)^2A_1$ (or $\tilde{B}\,^2A_1$) state is 3.97 eV above the $(2)^2A_1$ state at the CIS level of calculation. Since the minimum-energy geometry of the $\tilde{B}\,^2A_1$ state is at $r=1.6522$ Å and $\theta=132.3°$ [at the CASSCF/MRCI/aug-cc-pVQZ(no *g*) level; see Table I], there has to be an avoided crossing between these two $^2A_1$ states at $1.6522<r<2.572$ Å and $132.3>\theta>106.3°$, in agreement with the above MRCI results. With the electronic configuration of the neutral ground state of Cl_2O of $\cdots(9a_1)^2(3b_1)^2$, ionization to the $(2)^2A_1$ state of Cl_2O^+ is not allowed via a one-electron process. Nevertheless, intensity borrowing is possible via final state configuration interaction (CI) from the one-electron allowed $\tilde{B}\,^2A_1$ state. Qualitatively, the final state CI band arising from the ionization to the one-electron forbidden $(2)^2A_1$ cationic state is expected to be weak, but would have some effects on the observed PE spectrum of Cl_2O, particularly in the high ionization energy (IE) region of the $\tilde{B}\,^2A_1$ band. The diffuseness of the observed vibrational structure in the IE region of 12.5–12.8 eV, associated with the $\tilde{B}\,^2A_1$ PE band and underneath the $\tilde{C}\,^2A_2$ PE band, could well be due to the influence of ionization to the $(2)^2A_1$ state.

B. Optimized geometrical parameters, vibrational frequencies and AIEs

The computed minimum-energy geometrical parameters and vibrational frequencies obtained at different levels of calculation are summarized in Table II, the AIEs are summarized in Table III, and the T_e values of the excited cationic states relative to the $\tilde{X}\,^2B_1$ state are listed in Table IV. Included in these tables are available experimental and theoretical values for comparison. From Table II, the highest level calculations currently employed, for all states considered, to obtain equilibrium geometrical parameters are the RCCSD(T) calculations performed in the present study with either the cc-pVQZ or aug-cc-pVQZ basis sets, which give very similar values (within ≈0.002 Å and 0.08° in minimum energy bond lengths and angles) from geometry optimization calculations or the PEFs, respectively. For the $\tilde{X}\,^1A_1$ state of Cl_2O, the computed RCCSD(T)/aug-cc-pVQZ r_e and θ_e values agree with the available experimental values to within 0.009 Å and 0.08°, respectively. For the cationic states, the only available experimental geometrical parameters were derived from IFCA procedures carried out in our previous study, employing the harmonic oscillator model.[2] Revised IFCA geometrical parameters for each cationic state, obtained from the present study including anharmonicity, will be discussed later, when the simulated spectra are discussed below. In Table II, the computed fundamental frequencies of the symmetric stretching and bending modes obtained from the RCCSD(T)/aug-cc-pVQZ or CASSCF/MRCI/aug-cc-pVQZ(no *g*) PEFs are given together with the harmonic frequencies. In general, the computed fundamental frequencies agree better with available observed vibrational separations than the computed harmonic frequencies, as expected.

For each ionization, the calculated AIEs obtained at different levels of theory, shown in Table III for the four cationic states considered, appear to cover a reasonably wide range of values. For the $\tilde{X}\,^2B_1$, and $\tilde{C}\,^2A_2$ states, the observed AIE positions are well established from the He I PE spectrum. The experimental uncertainty in the measured ionization energy given in Ref. 1 is ±0.006 eV. However, in view of the instrumental energy resolution of about 20 meV quoted therein,[1] a more realistic uncertainty associated with

TABLE II. The computed equilibrium geometrical parameters (in Å and °) and harmonic vibrational frequencies (cm^{-1}) of the $\tilde{X}\,^1A_1$ state of Cl_2O and the $\tilde{X}\,^2B_1$, $\tilde{A}\,^2B_2$, $\tilde{B}\,^2A_1$, and $\tilde{C}\,^2A_2$ states of Cl_2O^+ at various levels of calculation.

State	Method	R(ClO)	θ(ClOCl)	ω_1	ω_2
$\tilde{X}\,^1A_1$	QCISD/6-31G*; opt[a]	1.730	111.31	654	300
	RCCSD(T)/aug-cc-pVTZ; PEF	1.715	110.85	642	293
	RCCSD(T)/cc-pVQZ; opt	1.705	110.87		
	RCCSD(T)/aug-cc-pVQZ; PEF	1.7045	110.81	651	298
	RCCSD(T)/aug-cc-pVQZ; PEF			646[b]	296[b]
	RCCSD(T)/TZ2P[c]	1.731	110.7	642	288
	RCCSD(T)/POL1[d]	1.757	110.7	615	280
	CAS-QPCI/cc-pVTZ[e]	1.7139	113.95	543	227
	CAS-QPCI/cc-pVTZ[f]	1.73	108.2		
	MP2/6-311+G(2df)[g]	1.7048	110.44		
	CCSD(T)/aug-cc-pVTZ[g]	1.7157	110.80		
	Expt[h]	1.69587	110.886	642	296
$\tilde{X}\,^2B_1$	QCISD/6-31G*; opt[a]	1.672	117.82	682	320
	RCCSD(T)/aug-cc-pVTZ; PEF	1.643	117.42	707	326
	RCCSD(T)/cc-pVQZ; opt	1.633	117.55		
	RCCSD(T)/aug-cc-pVQZ; PEF	1.6335	117.53	721	331
	RCCSD(T)/aug-cc-pVQZ; PEF			712[b]	330[b]
	MP2/6-311+G(2df)[g]	1.5903	118.05		
	CCSD(T)/aug-cc-pVTZ[g]	1.6504	117.28		
	IFCA(harm)[a]	1.640±0.004	117.3±0.3	678[i]	347[i]
	IFCA(anharm)	1.637	117.35		
$\tilde{A}\,^2B_2$	QCISD/6-31G*; opt[a]	1.726	94.84	750	279
	RCCSD(T)/aug-cc-pVTZ; PEF	1.716	91.03	717	299
	RCCSD(T)/cc-pVQZ; opt	1.706	90.92		
	RCCSD(T)/aug-cc-pVQZ; PEF	1.7054	90.84	729	305
	RCCSD(T)/aug-cc-pVQZ; PEF			724[b]	302[b]
	IFCA(harm)[a]	1.705±0.007	100.2±0.4		290[i]
	IFCA(anharm)	1.697	90.92		
$\tilde{B}\,^2A_1$	QCISD/6-31G*; opt[a]	1.671	132.41	562	284
	RCCSD(T)/aug-cc-pVTZ; PEF	1.628	132.01	647	294
	RCCSD(T)/cc-pVQZ; opt	1.621	132.20		
	CASSCF/MRCI/aug-cc-pVTZ(no g); PEF	1.6626	131.90	526	273
	CASSCF/MRCI/aug-cc-pVQZ(no g); PEF	1.6522	132.30	558	290
	CASSCF/MRCI/aug-cc-pVQZ(no g); PEF			544[b]	287[b]
	IFCA(harm)[a]	(1.637)	(131.99)		282[i]
	IFCA(anharm)	1.610	130.0		
$\tilde{C}\,^2A_2$	QCISD/6-31G*; opt[a]	1.739	108.87		
	RCCSD(T)/aug-cc-pVTZ; PEF	1.737	107.49	637	261
	RCCSD(T)/cc-pVQZ; opt	1.726	107.43		
	RCCSD(T)/aug-cc-pVQZ; PEF	1.7254	107.36	644	268
	RCCSD(T)/aug-cc-pVQZ; PEF			640[b]	268[b]
	IFCA(harm)[a]	1.725±0.004	108.9±0.5	613[i]	307[i]
	IFCA(anharm)	1.724	107.43		

[a]From Ref. 2.
[b]Fundamental frequencies from the computed PEFs.
[c]From Ref. 24.
[d]From Ref. 25.
[e]From multireference second-order quasidegenerate perturbation configuration interaction calculation of Ref. 4 and quoted in Ref. 5.
[f]From multireference second-order quasidegenerate perturbation configuration interaction calculation of Ref. 6.
[g]From a table in Ref. 9 [it is uncertain that the CCSD(T) calculations were performed in this work; the reference quoted in the text for the CCSD(T) calculations does not contain CCSD(T) calculations on Cl_2O or its cation].
[h]From Refs. 21 and 22; see also Ref. 1, and references therein.
[i]Fundamental frequencies from the He I photoelectron spectrum of Ref. 1.

the measured position of a vibrational component, particularly in regions with overlapping PE bands, is probably of the order of ±0.01 eV. Comparing the *ab initio* and observed AIEs for the $\tilde{X}\,^2B_1$ and $\tilde{C}\,^2A_2$ states, as shown in Table III, all the computed values employing large basis sets (QZ and 5Z) and the extrapolated values (to basis set limit) are consistently larger than the observed values. Ignoring the AIE values obtained with the relatively small aug-cc-pVDZ basis set, which are significantly smaller than those obtained with larger basis sets (by more than 0.25 eV), the averaged values of all the calculated AIEs for the $\tilde{X}\,^2B_1$ and $\tilde{C}\,^2A_2$ states, as shown in Table III, are 10.966 and 12.866 eV, respectively. These values are larger than the observed values[1] of 10.887 and 12.742 eV by 0.079 and 0.124 eV, respectively. Inclusion of the correction for zero-point-vibrational-energies, Δ(ZPVE), gives AIE values of 10.965 and 12.840 eV for the

TABLE III. Computed adiabatic ionization energies (eV) of the four lowest cationic states of Cl_2O obtained at different levels of calculations.

Methods	$\tilde{X}\,^2B_1$	$\tilde{A}\,^2B_2$	$\tilde{B}\,^2A_1$	$\tilde{C}\,^2A_2$
RCCSD(T)/cc-pVDZ//RCCSD(T)/cc-pVQZ	10.600	11.730	11.982	12.360
RCCSD(T)/cc-pVTZ//RCCSD(T)/cc-pVQZ	10.771	11.794	12.160	12.647
RCCSD(T)/cc-pVQZ//RCCSD(T)/cc-pVQZ	10.921	11.917	12.297	12.806
RCCSD(T)/cc-pV5Z//RCCSD(T)/cc-pVQZ	10.964	11.952	12.331	12.863
Extrapolation VTZ/VQZ Halkier *et al.*[a]	11.03	12.01	12.40	12.92
Extrapolation VQZ/V5Z Halkier *et al.*[a]	11.01	11.99	12.37	12.92
Extrapolation VDZ/VTZ Truhlar[b]	10.93	11.90	12.31	12.83
Extrapolation VDZ/V5Z $\{F(X)=BX^{-\alpha}\}$[c]	11.12	12.10	12.46	13.01
Extrapolation VDZ/V5Z $\{F(X)=BX^{-3}\}$[c]	10.95	11.93	12.32	12.86
Extrapolation VDZ/V5Z $\{F(X)=BX^{-\alpha X}\}$[c]	11.01	12.00	12.38	12.91
Extrapolation VTZ/VQZ Halkier *et al.*[d]	10.98	11.97	12.34	12.87
RCCSD(T)/aug-cc-pVTZ PEF	10.89	11.89	12.28	12.73
RCCSD(T)/aug-ccpVQZ PEF	10.97	11.95	⋯	12.84
RCCSD(T)/aug-cc-pVQZ//QCISD/6-31G*[e]	11.007	11.983	12.454	12.842
Average[f]	10.966	11.951	12.335	12.866
Average+Δ(ZPVE)[g]	10.965	11.958	12.320	12.840
Adjusted averaged values[h]	10.887	11.877	12.237	12.747
IFCA(harm)[e]	⋯	12.159	12.271	⋯
IFCA(anharm)	⋯	11.918	12.301	⋯
Experimental[i]	10.887	12.016	<12.453	12.742

[a]Two point extrapolation (see Ref. 11): $E_{\lim}=[X^{\alpha}/X^{\alpha}-(X-1)^{\alpha}]E_X-[(X-1)^{\alpha}/X^{\alpha}-(X-1)^{\alpha}]E_{X-1}$; E_X is the computed total electronic energy from the RCCSD(T)/cc-pVXZ calculation ($X=2,3,...$, for VDZ, VTZ,..., respectively, with VTZ≡cc-pVTZ etc.; similar for the rest in the table).

[b]Two point extrapolation (VDZ and VTZ data) (see Ref. 12): $E_{\lim}=[3^{\alpha}/(3^{\alpha}-2^{\alpha})]E_3^{\mathrm{HF}}-[2^{\alpha}/(3^{\alpha}-2^{\alpha})]E_2^{\mathrm{HF}}+[3^{\beta}/(3^{\beta}-2^{\beta})]E_3^{\mathrm{cor}}-[2^{\beta}/(3^{\beta}-2^{\beta})]E_2^{\mathrm{cor}}$.

[c]Energies fitted to (see Ref. 13): $E(X)=E_{\lim}+F(X)$.

[d]The vdz-v5z energies are fit to the following two equations (see Ref. 14): $E_{\mathrm{SCF}}(X)=E_{\mathrm{SCF}}+Be^{-\alpha x}$ and $E_{\mathrm{corr}}(X)=E_{\mathrm{corr\_}}+B'\,X^{-3}$.

[e]From Ref. 2.

[f]Averaged values of all the calculated values given above, except the RCCSD(T)/cc-pVDZ//RCCSD(T)/cc-pVQZ value.

[g]The averaged values (see footnote f) plus zero-point-vibrational-energy correction [Δ(ZPVE)]; computed vibrational energies from Ref. 2.

[h]Taking the experimental value of the first AIE and the T_0 values of the cationic states [the averaged values plus Δ(ZPVE) from Table IV]; see text.

[i]From Ref. 1.

$\tilde{X}\,^2B_1$ and $\tilde{C}\,^2A_2$ states respectively [averaged+Δ(ZPVE) in Table III; calculated harmonic vibrational energies used are from Ref. 2]. The effect of Δ(ZPVE) on the computed AIE for the $\tilde{X}\,^2B_1$ state is negligibly small, while that for the $\tilde{C}\,^2A_2$ state reduces the difference between the theoretical and experimental values slightly to 0.098 eV, which is still considerably larger than the realistic experimental uncertainty of ±0.01 eV mentioned above. In view of the computational efforts involved in obtaining the calculated AIEs, the above comparisons between the theoretical and observed values of the $\tilde{X}\,^2B_1$ and $\tilde{C}\,^2A_2$ states of Cl_2O^+ is slightly disappointing. Nevertheless, when the computed T_e values of the cationic states shown in Table IV are considered, the picture is more encouraging. The largest deviation of the calculated T_e values from the averaged value is only ±0.04 eV. The relative positions of the cationic states are very consistent at different levels of theory and hence should be reasonably reliable. Including ZPVE corrections to the computed T_e value of the $\tilde{C}\,^2A_2$ state, a T_0 value of 1.86 eV is obtained, which agrees with the observed separation between the AIE positions of the $\tilde{X}\,^2B_1$ and $\tilde{C}\,^2A_2$ states of 1.855 eV from Ref. 1 to within the realistic experimental uncertainty of ±0.01 eV. In view of this excellent agreement between the theoretical and experimental T_0 values, the first observed AIE was used together with the averaged T_e values plus Δ(ZPVE), i.e., averaged T_0 values, to give the adjusted averaged AIE values for the three excited cationic states (see Table III). The adjusted averaged AIE value for ionization to the $\tilde{C}\,^2A_2$ state of 12.747 eV agrees with the observed value of 12.742 eV to within 0.01 eV. Based on the above comparisons between theoretical and experimental relative energies of the $\tilde{C}\,^2A_2$ state, the uncertainties associated with the adjusted averaged AIE values for ionization to the $\tilde{A}\,^2B_2$ and $\tilde{B}\,^2A_1$ states is estimated to be ca. ±0.04 eV (the largest deviation of the calculated T_e values from the averaged T_e value for the $\tilde{C}\,^2A_2$ state). It is pleasing that the agreements between the final AIE values of these two cationic states obtained from spectral simulations to be discussed in the following subsection and the adjusted averaged values (see Table III and later text) are near this estimated uncertainty.

C. Spectral simulations

Different simulated PE bands are shown in Figs. 1–6, together with the experimental bands of Ref. 1, where appropriate, for comparison. In Fig. 1, the simulation of the first

TABLE IV. The computed T_e (eV) of the low-lying cationic states of Cl_2O^+ (with respect to the $\tilde{X}\,^2B_1$ state) obtained at different levels of calculations.

Methods	$\tilde{A}\,^2B_2$	$\tilde{B}\,^2A_1$	$\tilde{C}\,^2A_2$
RCCSD(T)/cc-pVDZ//RCCSD(T)/cc-pVQZ	1.130	1.382	1.760
RCCSD(T)/cc-pVTZ//RCCSD(T)/cc-pVQZ	1.023	1.389	1.876
RCCSD(T)/cc-pVQZ//RCCSD(T)/cc-pVQZ	0.993	1.376	1.885
RCCSD(T)/cc-pV5Z//RCCSD(T)/cc-pVQZ	0.988	1.367	1.899
Extrapolation VTZ/VQZ Halkier *et al.*[a]	0.99	1.37	1.89
Extrapolation VQZ/V5Z Halkier *et al.*[a]	0.98	1.36	1.91
Extrapolation VDZ/VTZ Truhlar[b]	0.97	1.38	1.90
Extrapolation VDZ/V5Z $\{F(X)=BX^{-\alpha}\}$[c]	0.98	1.34	1.89
Extrapolation VDZ/V5Z $\{F(X)=BX^{-3}\}$[c]	0.98	1.37	1.93
Extrapolation VDZ/V5Z $\{F(X)=BX^{-\alpha X}\}$[c]	0.99	1.37	1.90
Extrapolation VTZ/VQZ Halkier *et al.*[d]	0.99	1.36	1.89
RCCSD(T)/aug-cc-pVTZ PEF	1.000	1.390	1.840
RCCSD(T)/aug-ccpVQZ PEF	0.980	···	1.870
Averaged values[e]	0.99±0.02	1.37±0.02	1.89±0.04
Averaged values+Δ(ZPVE)[f]	0.99	1.35	1.86
IFCA (harm.)[g]	1.272	1.384	1.855[h]
IFCA (anharm.)	1.031	1.414	1.855[h]

[a]Two point extrapolation (see Ref. 11): $E_{\lim}=[X^\alpha/X^\alpha-(X-1)^\alpha]E_X-[(X-1)^\alpha/X^\alpha-(X-1)^\alpha]E_{X-1}$; E_X is the computed total electronic energy from the RCCSD(T)/cc-pVXZ calculation ($X=2,3,...$, for VDZ, VTZ,..., respectively, with VTZ≡cc-pVTZ etc.; similar for the rest in the table).

[b]Two point extrapolation (VDZ and VTZ data; see Ref. 12): $E_{\lim}=[3^\alpha/(3^\alpha-2^\alpha)]E_3^{\mathrm{HF}}-[2^\alpha/(3^\alpha-2^\alpha)]E_2^{\mathrm{HF}}+[3^\beta/(3^\beta-2^\beta)]E_3^{\mathrm{cor}}-[2^\beta/(3^\beta-2^\beta)]E_2^{\mathrm{cor}}$.

[c]Energies fitted to (see Ref. 13): $E(X)=E_{\lim}+F(X)$.

[d]The vdz-v5z energies are fit to the following two equations (see Ref. 13): $E_{\mathrm{SCF}}(X)=E_{\mathrm{SCF}}+Be^{-\alpha x}$ and $E_{\mathrm{corr}}(X)=E_{\mathrm{corr\_}}+B'X^{-3}$.

[e]The average values of all computed values given above, but excluding the RCCSD(T)/cc-pVDZ//RCCSD(T)/cc-pVQZ values; see text.

[f]Averaged values (see footnote e) plus Δ(ZPVE), i.e., T_0; see text.

[g]Reference 2.

[h]Experimental T_0 values from the separation of the AIEs of the first and fourth PE bands in the HE I photoelectron spectrum of Ref. 1.

PE band based on the harmonic oscillator model [Fig. 1(c)] from Ref. 2 is also included. The simulation which includes anharmonicity in each state [Fig. 1(b)] has employed the IFCA geometrical parameters, as given in Table II, which are very close to those obtained previously with the harmonic oscillator model[2] and the *ab initio* values. It can be seen that the anharmonic simulation is slightly superior to the harmonic one, when compared with the observed spectrum. In particular, the relative intensities of vibrational components in the bending series of the anharmonic simulation match better to those of the observed spectrum than the harmonic one. In the latter harmonic simulation, the (0,1,0) component is too strong, when compared with the observed spectrum. It should be noted that hot band contributions are included in all the simulations presented in this study assuming a Boltzmann distribution for the vibrational populations of the neutral molecule at a temperature of 300 K, as described previously.[2] Hot band contributions are clearly shown in the observed first PE band [Fig. 1(a)]. It will be shown that hot band contributions are significant, particularly in the $\tilde{A}\,^2B_2$, and $\tilde{B}\,^2A_1$ PE bands.

Figure 2 shows the simulated and observed PE spectra in the region of ≈12–13 eV, which consists of three overlapping PE bands of the $\tilde{A}\,^2B_2$, $\tilde{B}\,^2A_1$, and $\tilde{C}\,^2A_2$ states. The simulated PE bands of these three states have a relative intensity ratio of 0.255:0.22:0.88, respectively. This ratio was determined simply by matching the intensity of the strongest simulated vibrational component of each band to that of the corresponding observed strongest vibrational component. The available experimental geometrical parameters of the neutral molecule[21,22] and the IFCA geometrical parameters determined for the respective cationic states, as given in Table II, were employed to obtain the simulated spectrum. First, the simulated $\tilde{A}\,^2B_2\leftarrow\tilde{X}\,^1A_1$ band is considered. The IFCA geometrical parameters employed for the cationic state are actually those of the available experimental geometrical parameters of the neutral molecule plus the computed RCCSD(T)/aug-cc-pVQZ geometry change upon ionization. It appears that the *ab initio* geometry change to the $\tilde{A}\,^2B_2$ state, when combined with the available experimental neutral geometry, gives a simulated spectral band, which matches very well with the observed one, without any need of further adjustments of the geometrical parameters of the cationic state. The near exact match between the simulated and observed spectra for this state is shown more clearly in the expanded spectrum of Fig. 3, which also shows the bar diagrams of the major contributing vibrational series, including some hot band series. It can be seen in Figs. 2 and 3 that, for this PE band, the simulated vibrational component of maximum overall intensity is aligned to the observed peak of maximum intensity. This alignment gives the AIE position for the $\tilde{A}\,^2B_2\leftarrow\tilde{X}\,^1A_1$ ionization (indicated in Fig. 3) as 11.918 eV. This value obtained from the anharmonic simulation in the present study is 0.241 eV lower than the value

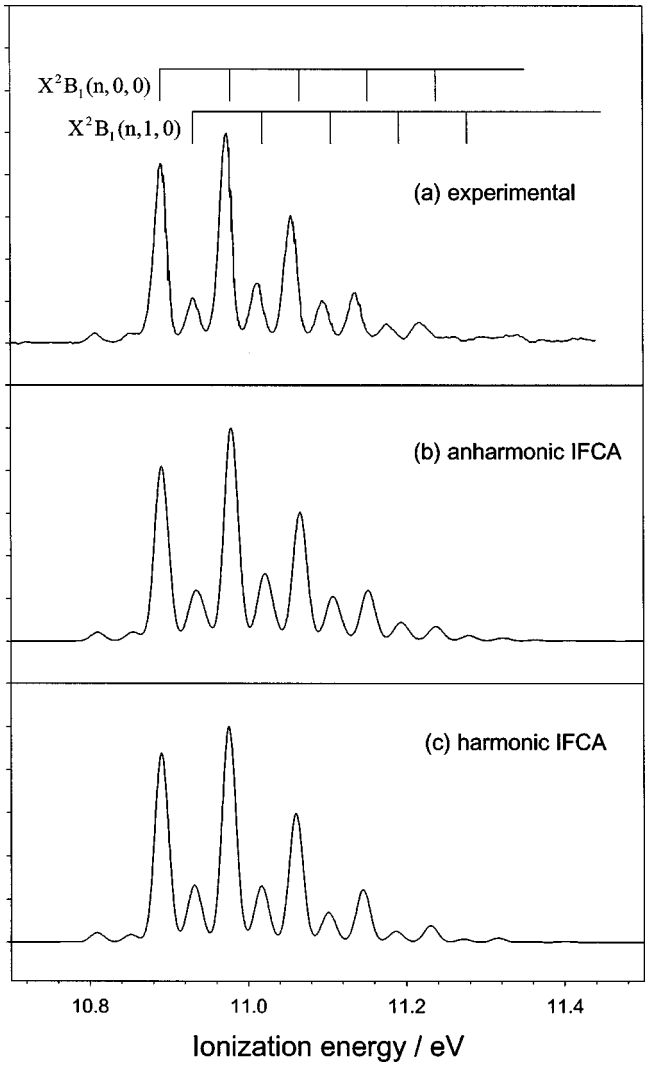

FIG. 1. The first band in the He I photoelectron spectrum of Cl_2O ($\tilde{X}\,^2B_1 \leftarrow \tilde{X}\,^1A_1$ ionization). (a) Experimental (from Ref. 1); (b) anharmonic simulation from the present study; and (c) harmonic simulation (from Ref. 2); see text.

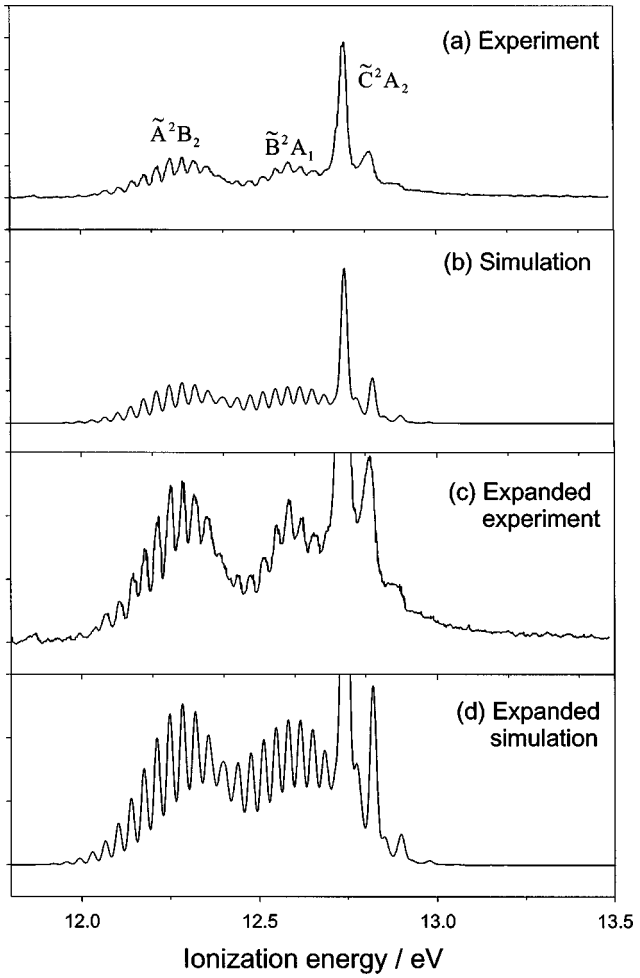

FIG. 2. The He I photoelectron spectrum of Cl_2O in the 12.0–13.0 eV region (consisting of the $\tilde{A}\,^2B_2$, $\tilde{B}\,^2A_1$, and $\tilde{C}\,^2A_2 \leftarrow \tilde{X}\,^1A_1$ ionizations). (a) Experimental (from Ref. 1); (b) anharmonic simulation from the present study; (c) experimental (expanded); and (d) anharmonic simulation (expanded); see text.

obtained previously employing the harmonic oscillator model,[2] but is between the averaged value and the adjusted averaged value from *ab initio* calculations (see Table III) discussed above. It is also within the theoretical uncertainty of ± 0.04 eV of the adjusted averaged value, as estimated above. It should be stressed that, for the simulation of this PE band associated with ionization to the $\tilde{A}\,^2B_2$ state, no empirical adjustment of the ionic state geometry via the IFCA procedure has been made to obtain the simulated spectrum, which gives an excellent match with the observed spectrum. This is in strong contrast to the best matching harmonic simulation, which has its ionic state IFCA geometrical parameters very different from the *ab initio* values (and the anharmonic IFCA values, particularly for the bond angle; see Table II). We will come back to this point on empirical adjustments later. Here, we just conclude that the IFCA geometrical parameters and the AIE value obtained from the anharmonic simulation for the $\tilde{A}\,^2B_2 \leftarrow \tilde{X}\,^1A_1$ ionization in the present study (Table II; Fig. 3 and Table III) should be currently the most reliable. In addition, similar to the second PE band of F_2O corresponding to ionization to the same cationic state,[3] both some hot bands and the adiabatic position are too weak to be observed (see Fig. 3). Nevertheless, hot band contributions, for example ionization from the (0,1,0) and (0,2,0) levels of the neutral state (Fig. 3), to the PE spectrum in the low IE region are significant and must be included in the simulation.

Before the third PE band corresponding to the $\tilde{B}\,^2A_1 \leftarrow \tilde{X}\,^1A_1$ ionization is discussed, we consider the fourth PE band corresponding to the $\tilde{C}\,^2A_2 \leftarrow \tilde{X}\,^1A_1$ ionization first. The IFCA geometrical parameters of the $\tilde{C}\,^2A_2$ state employed to give the simulated spectrum in Fig. 2 are very close to those obtained previously within the harmonic oscillator model and the *ab initio* values. Further slight adjustments in the geometrical parameters of the cationic state may give a better match between the simulated and observed spectra. However, it appears that this spectral region is poorly resolved because of underlying bands, which will be discussed below. Consequently, it is felt that further IFCA adjustments of the geometrical parameters of the cationic state are not justified, unless the spectrum is better resolved.

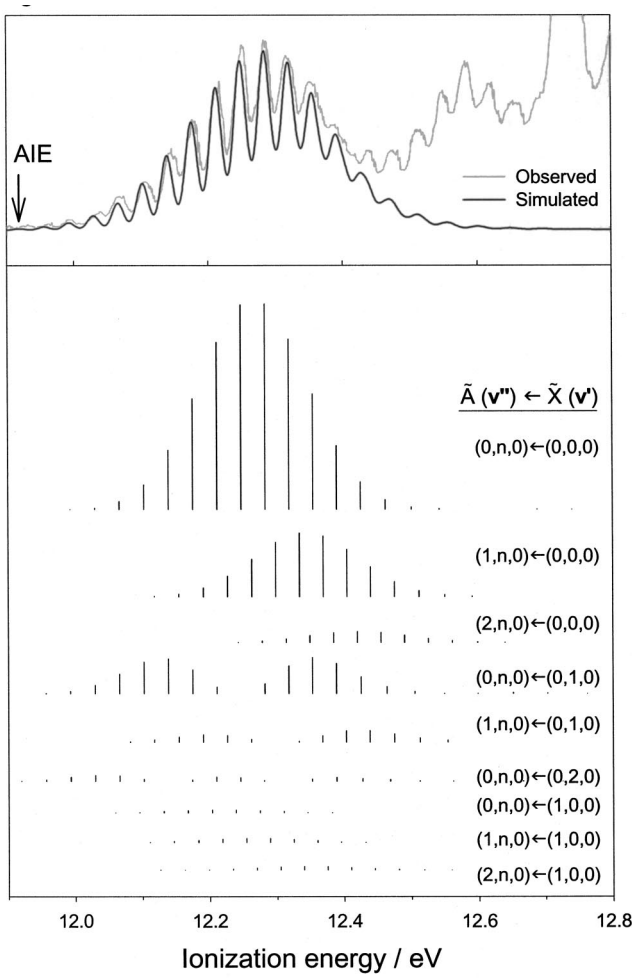

FIG. 3. The simulated and observed $\tilde{A}\,^2B_2 \leftarrow \tilde{X}\,^1A_1$ photoelectron bands, with the computed Franck–Condon factors of the vibrational series (including hot bands) with the strongest relative intensities given in bar diagrams; see text.

The uncertainties in the IFCA geometrical parameters of this state are, as a result, larger than those of the $\tilde{X}\,^2B_1$ and $\tilde{A}\,^2B_2$ states. However, the closeness of the IFCA and *ab initio* values suggests that they should be reasonably reliable.

For the $\tilde{B}\,^2A_1$ state, although the computed bond angles, θ_e, have very consistent values of $\approx$132.0° at different levels of calculation, the computed bond lengths, r_e, have values, which range from 1.621 to 1.671 Å (Table II). Based on the *ab initio* values shown in Table II, the trends in the computed r_e values with respect to levels of electron correlation and basis set variations can be summarized as follows. A higher level of theory (in terms of electron correlation and basis set size) yields a smaller value of r_e. Regarding the RCCSD(T)/cc-pVQZ and MRCI/aug-cc-pVQZ(no *g*) values, the former should be more accurate than the latter [provided that the T_1 diagnostic is acceptable in the RCCSD(T) calculations], as the RCCSD(T) method is size-consistent and also the basis sets employed is more complete. [The full cc-pVQZ basis set including g functions was employed in the RCCSD(T) calculations, while the diffuse part of the aug-cc-pVQZ(no *g*) basis set employed in the MRCI calculations should not be important at the equilibrium geometry, but would be important in regions away from the minimum.] It should also be noted that at the region of the equilibrium geometry, the T_1 diagnostics calculated in the RCCSD(T) calculations are acceptable and hence the RCCSD(T) method is superior to the MRCI method in the region of the minimum. In view of the above considerations, the r_e value computed at the RCCSD(T)/cc-pVQZ level of 1.621 Å may be considered as an upper limit of the true value.

The simulated PE band of the $\tilde{B}\,^2A_1 \leftarrow \tilde{X}\,^1A_1$ ionization, as shown in Figs. 2 and 4, has employed the ionic state, IFCA geometrical parameters of $r_e = 1.610$ Å and $\theta_e = 130.0°$. Aligning the strongest simulated vibrational component with the strongest observed component, the AIE position of the $\tilde{B}\,^2A_1 \leftarrow \tilde{X}\,^1A_1$ ionization, as indicated in Fig. 4, is at 12.301 eV. This AIE value is in between the averaged value and the adjusted averaged value from *ab initio* calculations (see Table III), and agrees with them and the value obtained previously from harmonic simulation[2] to within ca. ± 0.06 eV. Figure 5 shows a simulation similar to that of Fig. 4, but the IFCA geometrical parameters of the $\tilde{B}\,^2A_1$ state are $r_e = 1.6436$ Å [the MRCI r_e value of the $\tilde{B}\,^2A_1$ state plus the difference between the experimental r_e and the RCCSD(T)/aug-cc-pVQZ r_e of the neutral ground state] and $\theta_e = 123.0°$. The AIE value of the $\tilde{B}\,^2A_1 \leftarrow \tilde{X}\,^1A_1$ ionization from this simulation has a value of 12.476 eV. It can be seen from Figs. 2 and 5 that the simulated PE band of the $\tilde{B}\,^2A_1 \leftarrow \tilde{X}\,^1A_1$ ionization in Fig. 5 matches better the observed spectrum than that of Fig. 2. However, in order to obtain this better match, the IFCA bond angle of the cationic state takes a value, which is $\approx$10° smaller than the highly consistent *ab initio* value of 132.0°. At the same time, the AIE value thus obtained, is 0.239 eV higher than the adjusted averaged value from *ab initio* calculations. At present, it is felt that such a large geometry change in the IFCA procedure is not justified, though the simulated spectrum produced a better match with the observed spectrum. We will further discuss on this point below when we further consider the simulation of the $\tilde{A}\,^2B_2 \leftarrow \tilde{X}\,^1A_1$ PE band. For the $\tilde{B}\,^2A_1 \leftarrow \tilde{X}\,^1A_1$ band, the IFCA ionic bond angle of 130.0° employed in obtaining the simulated spectrum as shown in Figs. 2 and 4 should be regarded as the lowest reasonable limit for the θ_e value of the $\tilde{B}\,^2A_1$ state. The discrepancies between the simulated and observed $\tilde{B}\,^2A_1 \leftarrow \tilde{X}\,^1A_1$ band, as shown in Fig. 2, have to be due to some other factors, such as nonadiabatic coupling between the $\tilde{A}\,^2B_2$ and $\tilde{B}\,^2A_1$ states as considered by Mahapatra[10] and/or ionization to the one-electron forbidden $(2)^2A_1$ state via final state CI, discussed above.

Finally, it is felt that the effect of anharmonicity and the extent of the IFCA procedure on the simulated spectra should be further examined. The simulation of the $\tilde{A}\,^2B_2 \leftarrow \tilde{X}\,^1A_1$ band has been chosen for these purposes, because the nonadiabatic effect was found to be negligibly small for this band by Mahapatra.[10] Figure 6 shows the simulations of this PE band, employing harmonic and anharmonic FCFs and also different IFCA geometrical parameters for the $\tilde{A}\,^2B_2$ ionic state. The simulated spectrum in Fig. 6(d), employing anharmonic FCFs and the IFCA geometry from the present study, is identical to that in Fig. 3, which matches almost exactly

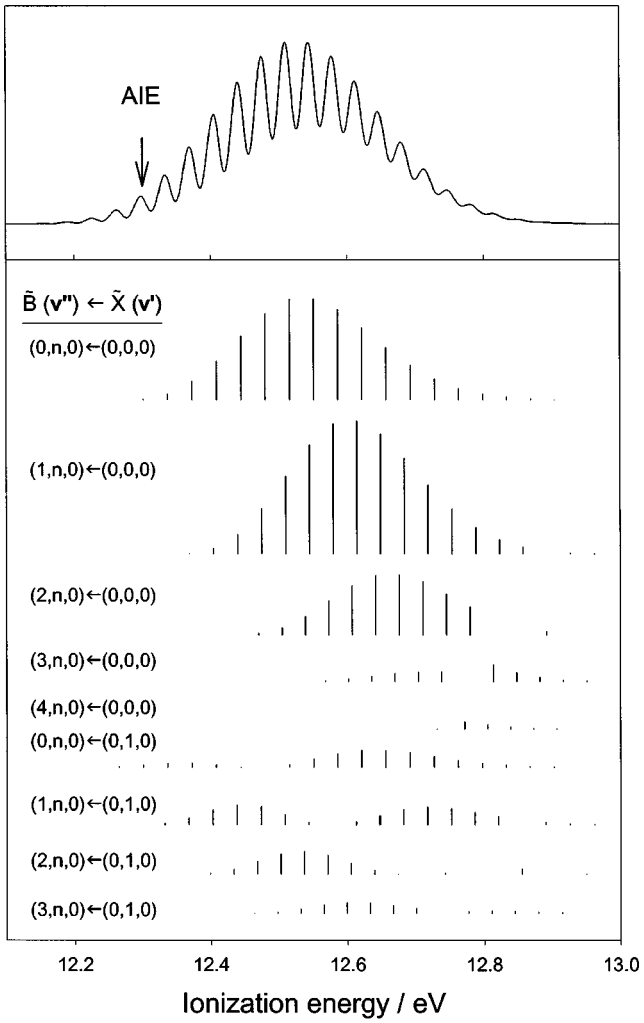

FIG. 4. The simulated $\tilde{B}\,^2A_1 \leftarrow \tilde{X}\,^1A_1$ photoelectron band and the computed Franck–Condon factors of the vibrational series (including hot bands) with the strongest relative intensities given in bar diagrams; the IFCA r_e and θ_e are 1.610 Å and 130.0°, respectively (see text).

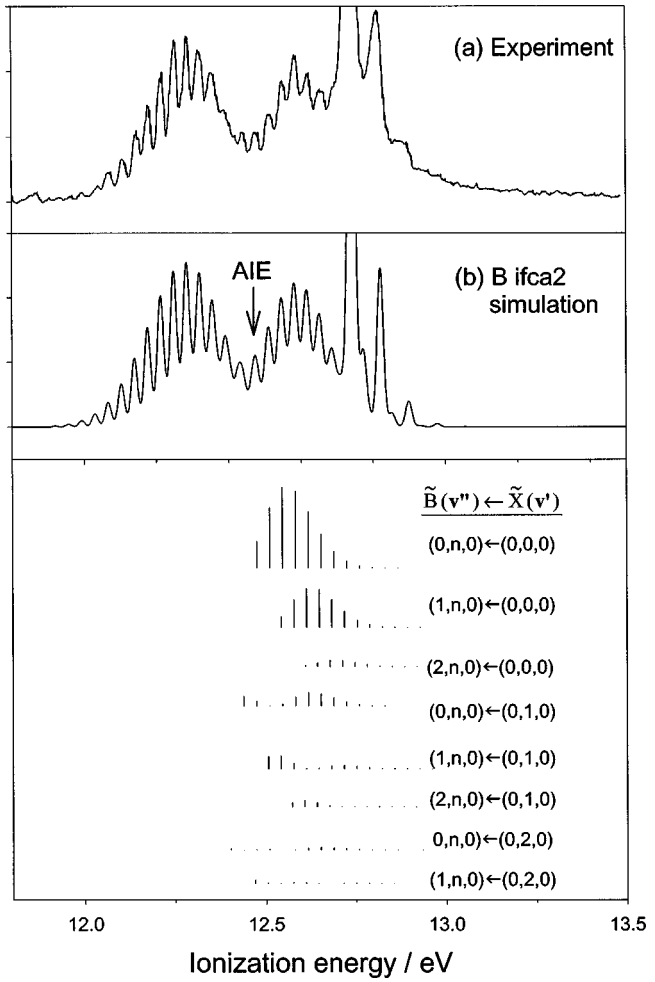

FIG. 5. The experimental and simulated photoelectron band as in Figs. 2(c) and 2(d), but the IFCA r_e and θ_e for the $\tilde{B}\,^2A_1$ state are 1.6436 Å and 123.0°, respectively (see text); the computed Franck–Condon factors of the vibrational series (including hot bands) with the strongest relative intensities are given in bar diagrams for the $\tilde{B}\,^2A_1$ PE band.

the observed spectrum (see Fig. 3). It can be seen that employing harmonic FCFs with the same IFCA geometry (obtained including anharmonicity) from the present study gives a simulated PE band shown in Fig. 6(a), which is considerably broader than the one employing anharmonic FCFs [Fig. 6(d)]. Figure 6(b) shows the harmonic simulation employing the QCISD/6-31G* geometry for the $\tilde{A}\,^2B_2$ ionic state (from Ref. 2) and it is also significantly broader than that of Fig. 6(d). These comparisons clearly demonstrate the importance of including anharmonicity in the simulation.

Figure 6(c) is a harmonic simulation, employing the IFCA ionic state geometrical parameters of $r_e = 1.705$ Å and $\theta_e = 97.0°$ and an AIE of 12.071 eV. This is the best match with the observed spectrum with harmonic FCFs. The main difference between this simulation and that reported in Ref. 2 is that, the latter assumes that the first simulated vibrational component is the first observable one, while the former just aligns the vibrational component with the maximum simulated intensity to that with the maximum observed intensity. Comparing Figs. 6(c) and 6(d), it can be seen that even employing harmonic FCFs it is possible to produce a simulated PE band, which has a bandwidth similar to that of the observed spectrum. However, the IFCA θ_e value is now 97.0°, 7° larger than that obtained from the anharmonic IFCA procedure and the highly consistent *ab initio* values of ≈90.1° (see Table II). The conclusion drawn from this comparison is that excessive adjustments of geometrical parameters in the IFCA procedure are strongly undesirable. In this connection, reliable *ab initio* geometrical parameters obtained from high-level calculations, on which the IFCA procedure is based, are of paramount importance and the IFCA deviations from consistent and hence reliable *ab initio* values should be within 0.02 Å and 2.0° for r_e and θ_e, respectively.

IV. CONCLUDING REMARKS

Near state-of-the-art level PEFs, geometrical parameters, anharmonic vibrational wave functions, and AIE/T_e values of the four lowest lying cationic states of Cl_2O have been reported. Based on spectral simulations including anharmonicity, revised AIE values and/or equilibrium geometrical parameters have been obtained for some of these states. It was found that the inclusion of anharmonicity in the evaluation of

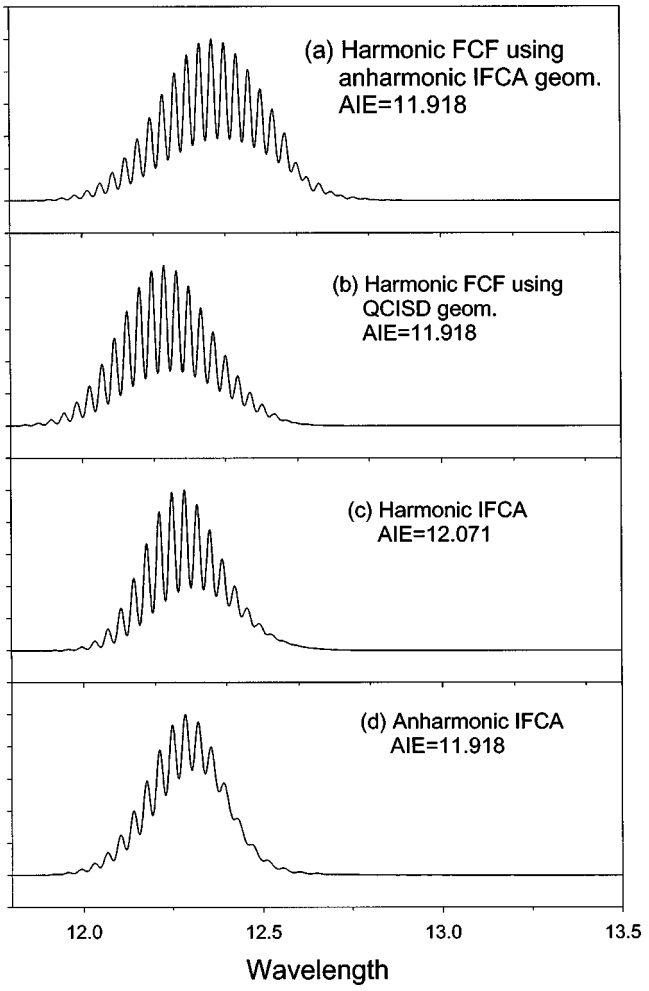

FIG. 6. The simulated $\tilde{A}\,^2B_2 \leftarrow \tilde{X}\,^1A_1$ photoelectron band: (a) using harmonic FCFs, the anharmonic IFCA geometry (1.697 Å; 90.92°) and the AIE value of 11.918 eV; (b) using harmonic FCFs, the QCISD/6-31G* geometry (1.726 Å; 94.84° from Ref. 2) and the AIE value of 11.918 eV; (c) using harmonic FCFs, the harmonic IFCA geometry (1.705 Å; 97.0°) and the AIE value of 12.071 eV; and (d) using anharmonic FCFs, the anharmonic IFCA geometry (1.697 Å; 90.92°) and the AIE value of 11.918 eV (same as Fig. 3); see text.

FCFs is important, particularly for the PE band associated with the $\tilde{A}\,^2B_2 \leftarrow \tilde{X}\,^1A_1$ ionization. However, for the $\tilde{B}\,^2A_1 \leftarrow \tilde{X}\,^1A_1$ ionization, it appears that even inclusion of anharmonicity could not yield a satisfactory simulated spectrum, when compared with the observed spectrum, unless excessive adjustment of the θ_e value of the cationic state is made in the IFCA procedure. It is therefore concluded that the discrepancies between the simulated and observed $\tilde{B}\,^2A_1 \leftarrow \tilde{X}\,^1A_1$ PE bands are probably partly due to the $(2)^2A_1$ surface which crosses the $\tilde{B}\,^2A_1$ state surface at a certain region and partly due to nonadiabatic coupling between the $\tilde{A}\,^2B_2$ and $\tilde{B}\,^2A_1$ states, as considered by Mahapatra.[10]

At this point, some comments on the related work of Mahapatra[10] seem appropriate. First, it is clear that the simulated spectrum, which includes nonadiabatic effects reported by Mahapatra, matches very well with the observed spectrum. Our study here including anharmonicity also supports the conclusion of Mahapatra that nonadiabatic effects are probably important for the $\tilde{B}\,^2A_1 \leftarrow \tilde{X}\,^1A_1$ PE band. However, it should be noted that Mahapatra has employed the harmonic oscillator model in the treatment of the vibrational motion and we have shown in the present study that anharmonicity is important. Specifically, including anharmonicity has reduced the bandwidth of the $\tilde{A}\,^2B_2 \leftarrow \tilde{X}\,^1A_1$ PE band considerably [see Figs. 6(a) and 6(d)]. In addition, we have also shown that hot band contributions are significant and should be included in the simulation, but Mahapatra has not included hot bands in his work. As hot bands are clearly identified in the observed first PE band, because of population of low-lying vibrational levels in the neutral molecule at room temperature, it is not consistent to ignore them in the higher bands. The inclusion of hot bands in the simulation of a PE band would particularly affect the AIE position obtained from the comparison between the simulated and observed spectra.

Finally, it should be emphasized that extra care should be taken in a simulation study, where some parameters are adjusted empirically so as to obtain the best match between the simulated and observed spectra. We have shown that, with excessive adjustments of some geometrical parameters, the IFCA procedure can produce a simulated spectrum, which matches the observed one, even employing the harmonic oscillator model [see Figs. 6(c) and 6(d)]. Obviously such a good match is fortuitous. In this connection, the excellent match between the simulated spectrum of Mahapatra for the $\tilde{B}\,^2A_1 \leftarrow \tilde{X}\,^1A_1$ band and the observed spectrum has to be viewed with caution, as there are at least three parameters (λ, τ, and κ; see Ref. 10 for detail), which have been adjusted empirically in order to obtain the simulated spectrum which matches best with the experimental spectrum. Reliable values of these parameters obtained via some means other than empirical adjustments would help to assess the justifiability of the empirical adjustments of these values and hence also assess the true extent of the ionic state nonadiabatic effects on the simulated spectrum. In the present study, geometrical parameters obtained at near state-of-the-art *ab initio* levels have been compared to values obtained by reasonable empirical adjustments of the geometrical parameters of the cationic state in the IFCA procedure, which lead to a good fit with an experimental envelope. In view of the above considerations, the AIE value of 12.171 eV estimated in the work of Mahapatra[10] for the $\tilde{B}\,^2A_1$ state is almost certainly less reliable than the IFCA value of 12.301 eV and the adjusted averaged *ab initio* value of 12.237 eV obtained in the present investigation.

In summary, the four PE bands, which appear in the He I PE spectrum of Cl_2O, have been simulated by combining *ab initio* calculations with FC calculations. Simulations of the first, second, and fourth bands agree well with the experimental envelope and in each case, recommendations can be made for the AIE value and the ionic state equilibrium geometry. For the third PE band, an AIE value of 12.30 ± 0.06 eV can be recommended. However, simulations of the FC envelope differ from the experimental envelope because of interaction between the $\tilde{B}\,^2A_1$ and $2\,^2A_1$ state and because of nonadiabatic coupling between the $\tilde{A}\,^2B_2$ and $\tilde{B}\,^2A_1$ states,

which has a negligible effect on the band envelope of the second band corresponding to the $\tilde{A}\,^2B_2 \leftarrow \tilde{X}\,^1A_1$ ionization.

ACKNOWLEDGMENTS

The authors are grateful to the Research Grant Council (RGC) of the Hong Kong Special Administrative Region (Projects Nos. POLYU 5187/00P and 5298/01P) and the Research Committee of the Hong Kong Polytechnic University (Project code: G-YY31). Support from the EPSRC(UK) and the Leverhulme Trust is also acknowledged.

[1] F. Motte-Tollet, J. Delwiche, J. Heinesch, M. J. Hubin-Franskin, J. M. Gingell, N. C. Jones, N. J. Mason, and G. Marston, Chem. Phys. Lett. **284**, 452 (1998).
[2] D.-C. Wang, E. P. F. Lee, F.-T. Chau, D. K. W. Mok, and J. M. Dyke, J. Phys. Chem. A **104**, 4936 (2000).
[3] D.-C. Wang, F.-T. Chau, D. K. M. Mok, E. P. F. Lee, L. Beeching, J. S. Ogden, and J. M. Dyke, J. Chem. Phys. **114**, 10682 (2001).
[4] A. Toniolo, M. Persico, and D. Pitea, J. Phys. Chem. A **104**, 7278 (2000).
[5] P. Tomasello, M. Ehara, and H. Nakatsuji, J. Chem. Phys. **116**, 2425 (2002).
[6] C. Collaveri, G. Granucci, M. Persico, and A. Toniolo, J. Chem. Phys. **115**, 1251 (2001).
[7] K. L. Baluja, N. J. Mason, L. A. Morgan, and J. Tennyson, J. Phys. B **34**, 2807 (2001).
[8] E. Ruhl, U. Rockland, H. Baumgartel, O. Losking, M. Binnewies, and H. Willner, Int. J. Mass. Spectrom. **187**, 545 (1999).
[9] G. Hanel, J. Fedor, B. Gstir, M. Probst, P. Scheier, T. D. Mark, T. Tegeder, and N. J. Mason, J. Phys. B **35**, 589 (2002).
[10] S. Mahapatra, J. Chem. Phys. **116**, 8817 (2002).
[11] A. Halkier, T. Helgaker, W. Klopper, P. Jorgensen, and A. G. Csaszar, Chem. Phys. Lett. **310**, 385 (1999).
[12] D. G. Truhlar, Chem. Phys. Lett. **294**, 45 (1998).
[13] D. Feller and K. A. Peterson, J. Chem. Phys. **108**, 154 (1998).
[14] A. Halkier, T. Helgaker, P. Jorgensen, W. Klopper, H. Koch, J. Olsen, and A. K. Wilson, Chem. Phys. Lett. **286**, 243 (1998).
[15] MOLPRO is a package of *ab initio* programs written by H.-J. Werner and P. J. Knowles, with contributions from J. Almlöf, R. D. Amos, A. Berning *et al.*
[16] S. Carter and N. C. Handy, J. Chem. Phys. **87**, 4294 (1987).
[17] J. E. Dennis, Jr., D. M. Gay, and R. E. Welsh, ACM Trans. Math. Softw. **7**, 348 (1981); **7**, 369 (1981).
[18] J. K. G. Watson, Mol. Phys. **19**, 465 (1970).
[19] D. W. K. Mok, E. P. F. Lee, F.-T. Chau, D.-C. Wang, and J. M. Dyke, J. Chem. Phys. **113**, 5791 (2000).
[20] F.-T. Chau, J. M. Dyke, E. P. F. Lee, and D. K. W. Mok, J. Chem. Phys. **115**, 5816 (2001).
[21] M. Nakata, M. Sugic, H. Takeo, C. Matsumura, T. Fukuyama, and K. Kuchitsu, J. Mol. Spectrosc. **86**, 241 (1981).
[22] G. E. Herberich, R. H. Jackson, and D. J. Millen, J. Chem. Soc. A **3**, 366 (1966).
[23] M. J. Frisch, G. W. Trucks, H. B. Schlegel *et al.*, GAUSSIAN 98, Gaussian, Inc., Pittsburgh, PA, 1998.
[24] T. J. Lee, J. Phys. Chem. **98**, 3687 (1994).
[25] J. E. Del Bene, J. D. Watts, and R. J. Bartlett, Chem. Phys. Lett. **246**, 541 (1995).